JOURNAL OF THEORETICAL AND APPLIED MECHANICS
60, 4, pp. 625-635, Warsaw 2022
https://doi.org/10.15632/jtam-pl/153011

STUDY ON THE SHEAR CREEP CHARACTERISTICS OF ANCHORED JOINTED ROCK MASSES UNDER CREEP FATIGUE LOADING

Yang Song
Department of Architecture and Transportation, Liaoning Technical University, Fuxin, Liaoning Province, China
Yong-Qi Li
School of Civil and Transportation Engineering, Hebei University of Technology, Tianjin, China
e-mail: 202111601014@stu.hebut.edu.cn

To study creep characteristics of deep rock masses under low-frequency earthquakes and other loads, sandstone and marble samples were used to characterize soft rock and hard rock, respectively. Shear creep tests of anchored rock masses under fatigue loading were carried out by using the graded loading method. A new nonlinear rheological model was constructed to characterize mechanical properties of anchored rock masses under fatigue loading. Creep fatigue curves of soft rock and hard rock have clear creep characteristics including instantaneous, attenuation, steady-state and accelerated creep stages. This work provides new insights into the stability of rock masses.

Keywords: disturbed load, sandstone, marble, creep body, rheological model

1. Introduction

The engineering geological conditions of deep jointed rock masses are extremely complex, and the mechanical interaction between bolts and jointed rock masses is difficult to accurately grasp, which leads to deformation and instability of jointed rock masses. With the construction of large-scale strategic projects in deep rock masses in China, safety and stability of underground engineering is of great importance (Feng *et al.*, 2022; Wiatowski *et al.*, 2021). The complex engineering geological environment poses many challenges to the development of underground engineering, in which the influence of load on deep rock masses cannot be ignored (Szkudlarek and Janas, 2021).

Related experts have carried out a series of studies on creep loads encountered in geotechnical engineering: Huang *et al.* (2017) carried out a uniaxial creep test on soft rock and built a creep constitutive model suitable for soft rock based on the concept of a disturbance. Luo *et al.* (2020) described creep characteristics of frozen sand. Based on the coupling relationship between strain and time, a creep constitutive model was established to describe the sand. Hu *et al.* (2019) carried out creep tests on fractured hard rock under high stress in deep areas. Wang *et al.* (2014) proposed a new rheological element with damage induced by high temperatures by studying creep characteristics at different temperatures. Wei *et al.* (2019) carried out cyclic uniaxial compression loading and unloading experiments of marble under different upper stress limits and numbers of cycles. Zhu *et al.* (2016) carried out uniaxial graded cyclic loading and unloading tests of coal rock combinations and explored creep characteristics of coal rock combinations under cyclic loading and unloading.

The above-mentioned research mainly analyzed the influence of creep load or cyclic load on the stability of deep rock masses (Sun, 2007; Yu *et al.*, 2014; Zuo *et al.*, 2019). In practical engineering, deep rock masses undergo creep deformation for a long time after excavation and support. When subjected to seismic load, the cyclic load will accumulate on the basis of the creep

load. At present, there are few studies on this engineering phenomenon. Based on the above engineering disaster phenomenon, this paper mainly studies failure characteristics of anchored deep rock masses under blasting or disturbance loads and establishes a constitutive model by introducing nonlinear creep to quantitatively analyze mechanical characteristics of specimens and provide a theoretical basis for the stability of anchored rock masses.

2. Creep tests under fatigue loading

2.1. Specimen making

To study shear creep characteristics of anchored soft and hard rock masses under fatigue loading, sandstone and marble are selected as representative soft rock and hard rock, respectively, and their conventional mechanical parameters are shown in Table 1.

Table 1. Conventional mechanical parameters of rock mass

Rock	Compressive strength [MPa]	Tensile strength [MPa]	Shear modulus [GPa]	Poisson's ratio	Cohesion [MPa]	Internal friction angle
Sandstone	22.10	1.25	8.83	0.23	8.31	36.12
Marble	100.63	3.59	21.21	0.25	15.22	22.50

Each anchored jointed rock mass specimen is 100 mm×100 mm×50 mm (Jierula *et al.*, 2021; Nádudvari *et al.*, 2021). The size of the specimen conforms to the relevant provisions of the International Society of Rock Mechanics test code, and the manufacturing steps are as follows:

(1) Rock block processing: A massive rock mass is selected, and a rock cutting machine is used to process the rock block into a 100 mm×100 mm×50 mm rock mass. A drilling machine is used to drill a hole with a diameter of 10 mm and a length of 50 mm at the center of the 100 mm×100 mm side as a reserved hole for the anchor rod.
(2) Rock block bonding: The upper and lower plates of the rock block are bonded by joints, and the joint part is filled with cement mortar to form a 100 mm×100 mm×5 mm cuboid; the mix proportions of the mortar are cement: medium river sand: water = 1 : 1.5 : 0.8, and 42.5 ordinary Portland cement is used (Małkowski *et al.*, 2021).
(3) Anchor rod installation: HRB335 steel is used as the anchor material, and the yield strength is 335 MPa. The reinforcement with a diameter of 6 mm is installed into the reserved hole of the test piece, and the overall length of the reinforcement is 110 mm. One end of the ribbed reinforcement is machined with a thread with a length of 10 mm, and the other side is placed 50 mm deep in the upper and lower plates. Grouting is used to fill this hole and the holes created to reinforce the anchor rod. The grouting material is the same as the joint material.

A specimen made according to the above steps is shown in Fig. 1.

2.2. Test procedure

The test instrument is shear equipment of the TAW-2000 rock servo machine in the Civil Engineering Test Center of Liaoning University of Engineering and Technology (Jangara and Ozturk, 2021; Szkudlarek and Janas, 2021). The shear stress is divided into five grades. Shear testing without the side limit is performed here, and a control group is included to provide data from the testing performed without a fatigue load. The test steps are as follows:

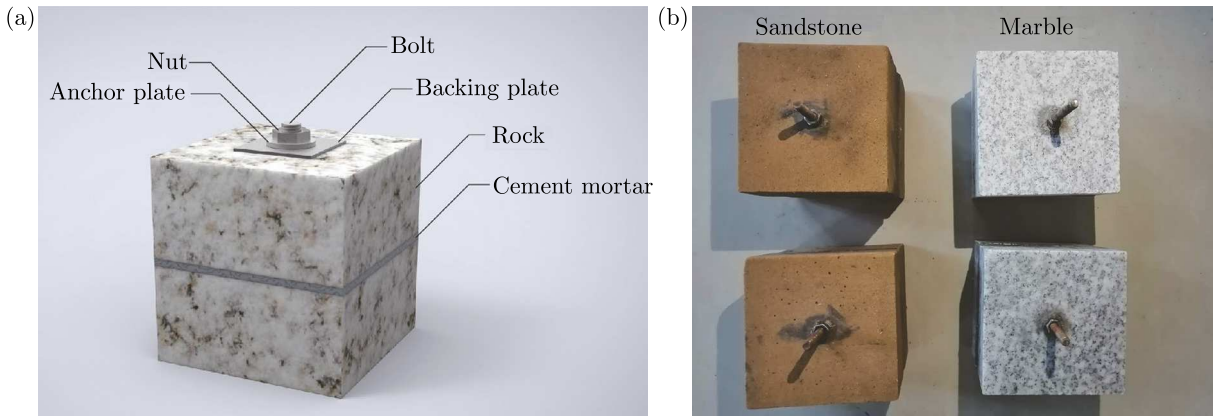

Fig. 1. Model diagram: (a) model diagram, (b) physical model

(1) Apply the shear stress: The test piece is placed into the shear device, the loading rate is control to 0.5 MPa/s, and incrementally higher horizontal shear stresses are applied. In each stage, the load is kept constant, and the instantaneous shear displacement is measured and read immediately. The extensometer was used to measure the shear displacement in this test.

(2) Apply the fatigue load: When the shear stress level corresponding to each stage is applied for approximately 50 h, the fatigue load is applied at the loading and unloading rate of 200 N/s (Małkowski *et al.*, 2021; Valiulin *et al.*, 2020), and the load level is increased by 5 kN from this stage. Then, the load level is repeatedly reduced by 5 kN until the fatigue loading period is complete. Three cycles of fatigue loading are applied during each stage. The shear stress corresponding to 5 kN of the converted fatigue load is 0.5 MPa. The specific load application is shown in Fig. 2. The fatigue frequency is 0.01 Hz. Notably, after the fatigue load is applied, the load is maintained for a certain period of time to adjust the internal stress of the test piece to make it more in line with actual engineering practice.

(3) Read the deformation data: The attenuation and steady-state shear creep data are read at intervals of 5 min, 10 min, 20 min, 40 min, 1 h, 2 h, 4 h, 8 h and 12 h. After that, the deformation data are read every 12 hours. Notably, when the fatigue load is applied to the specimen, the deformation data are read every 0.5 min. The condition of stable shear creep deformation of a rock mass is that the creep rate increment is $\leqslant 5 \cdot 10^{-4}$ mm/d (Song *et al.*, 2020); the accelerated creep stage is characterized by a large creep deformation and a faster creep rate, and in this stage, the deformation data are read every 5 min until the specimen is damaged.

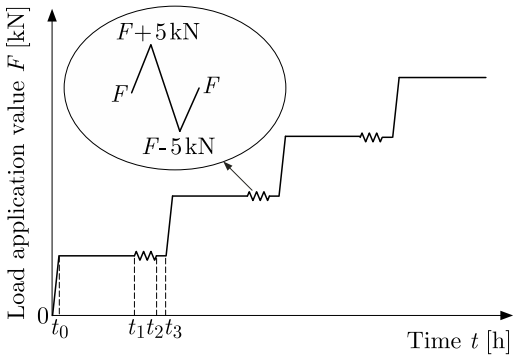

Fig. 2. Loading path diagram

Note: the period 0-t_1 in the figure is the loading time before reaching the specified load; t_1-t_2 is the stability time of the specified load; t_1-t_2 is the fluctuation time of the applied fatigue load; t_2-t_3 is the stabilization time after fatigue loading.

3. Analysis of test results

3.1. Test curve analysis

Through sorting and analyzing the test data, the data with typical creep curve characteristics are selected and plotted as shown in Fig. 3. In this study, the shear strain is the relative deformation caused by two parallel shear forces acting in opposite directions on the upper and lower parts of the specimen.

Figure 3 illustrates the following results:

(1) The creep strain curve and creep fatigue strain curve show clear creep deformation characteristics which include instantaneous creep, decay creep, steady creep and accelerated creep deformation. At the same time, the creep deformation induced with the fatigue load is greater than that without the fatigue load and increases with an increase in the shear stress. The creep failure deformation of sandstone and marble increases by 12.8% and 21.9%, respectively, with the fatigue load relative to that without the fatigue load, which indicates that the hard rock deformation is more sensitive to fatigue loading.

(2) The comparison of the soft and hard rock deformation under fatigue loading shows that the creep deformation of sandstone is greater than that of marble, and the final creep deformation of sandstone is approximately 1.6 times that of marble, which indicates that the rheological properties of a specimen with low strength are more obvious than those with high strength.

(3) With the increase in shear stress, the growth in creep with the fatigue load presents a gradually decreasing trend, which is due to internal pores of the specimen closing gradually in the steady-state stage. This change reduces the influence of fatigue load on creep of the specimen, consequently, decreasing the increase in creep.

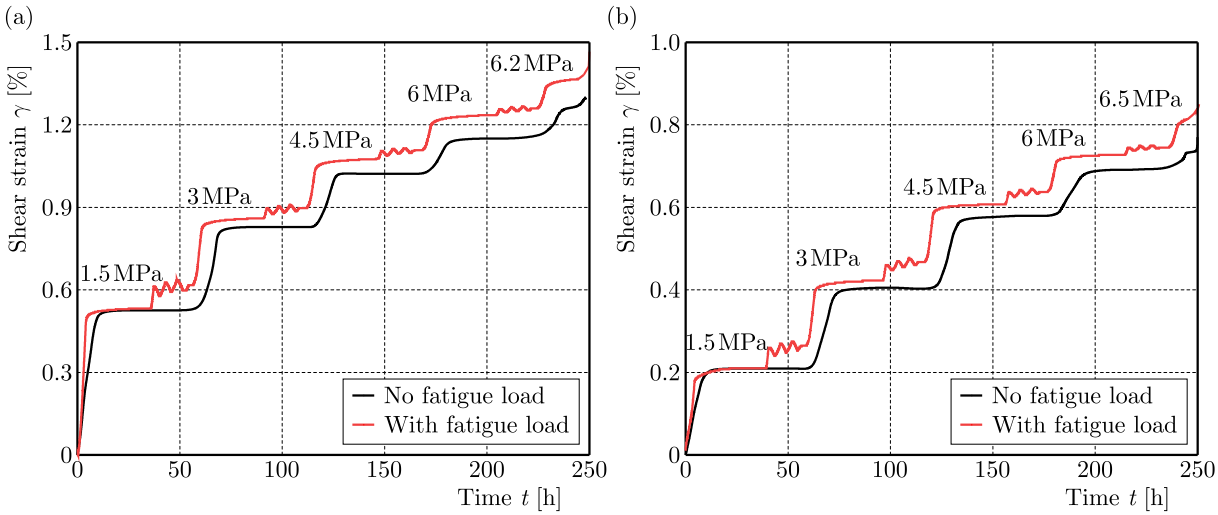

Fig. 3. Test curves: (a) sandstone, (b) marble

3.2. Isochronal shear stress-strain curves

To determine the shear strength of a specimen by using the Boltzmann (Jangara and Ozturk, 2021) superposition principle and the data in Fig. 3, isochronal shear stress-strain curves of different rock specimens are drawn with the results from each stage for each time interval, as shown in Fig. 4.

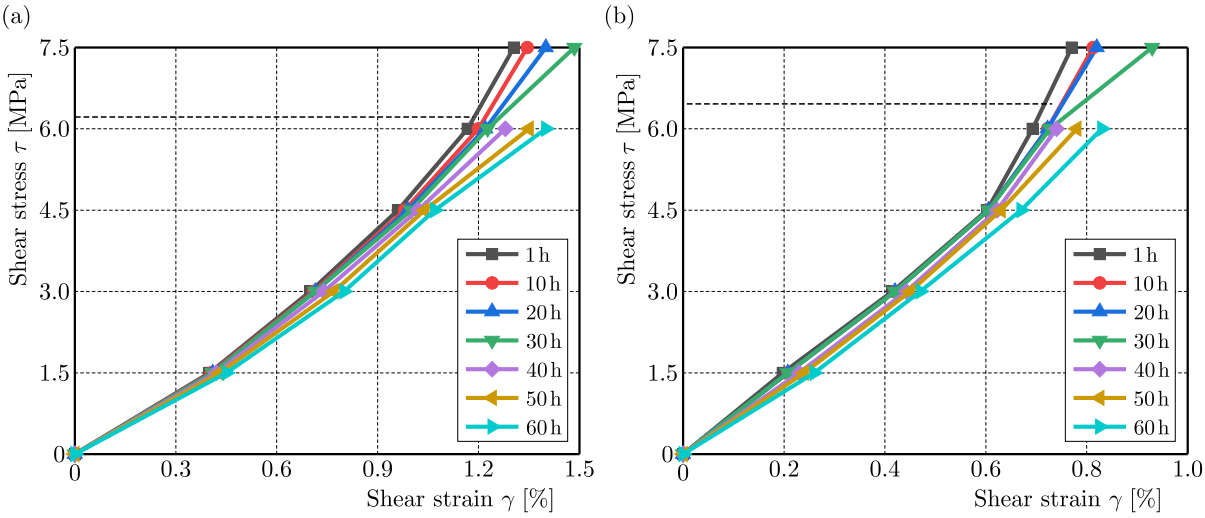

Fig. 4. Isochronal shear stress-strain curves under fatigue loading: (a) sandstone, (b) marble

Figure 4 shows that the shear strength of different rock specimens are different. The shear strength of sandstone and marble is 6.2 MPa and 6.5 MPa, respectively. The isochronal shear stress-strain curves are basically the same and are almost straight lines. With an increase in shear stress, the original internal pores of a rock specimen close while new cracks form and propagate. If the slope is defined as the isochronal shear modulus decreases with an increase in time for the same rock strength; additionally, the isochronal shear modulus increases with an increase in specimen strength. That is, the isochronal shear modulus of the marble is higher than that of the sandstone because the increase in rock strength improves the ability of a specimen to resist shear deformation; thus, a higher shear stress is required to induce the same shear deformation.

3.3. Residual strength analysis

To better study the ability of a specimen to resist shear deformation, the shear stress-strain curves of the rock specimens under fatigue loading are drawn, as shown in Fig. 5.

Figure 5 shows that with an increase in the shear stress, the shear strain presents an approximately linear deformation trend. When the shear stress is stable at a certain level, the deformation does not change at a low stress level but increases slightly at a high stress level, which is reflected as a short horizontal line in the figure. When the fatigue load is applied, the shear stress-strain curve forms an open loop. With an increase in the applied shear stress, the area of the hysteresis loop caused by fatigue loading decreases, and in the figure, the loops of the curve become increasingly dense. When the shear stress increases, the specimen ultimately reaches its shear strength. Due to the combined action of creep loading and fatigue loading, the internal cracks of the specimen expand and develop rapidly, which leads to a rapid decline in the shear deformation resistance. Due to friction of the joint surface, the specimen still has a certain shear strength. The corresponding stable shear strength is the residual strength, and the residual strength of sandstone is higher than that of marble, approximately 1.5 times higher.

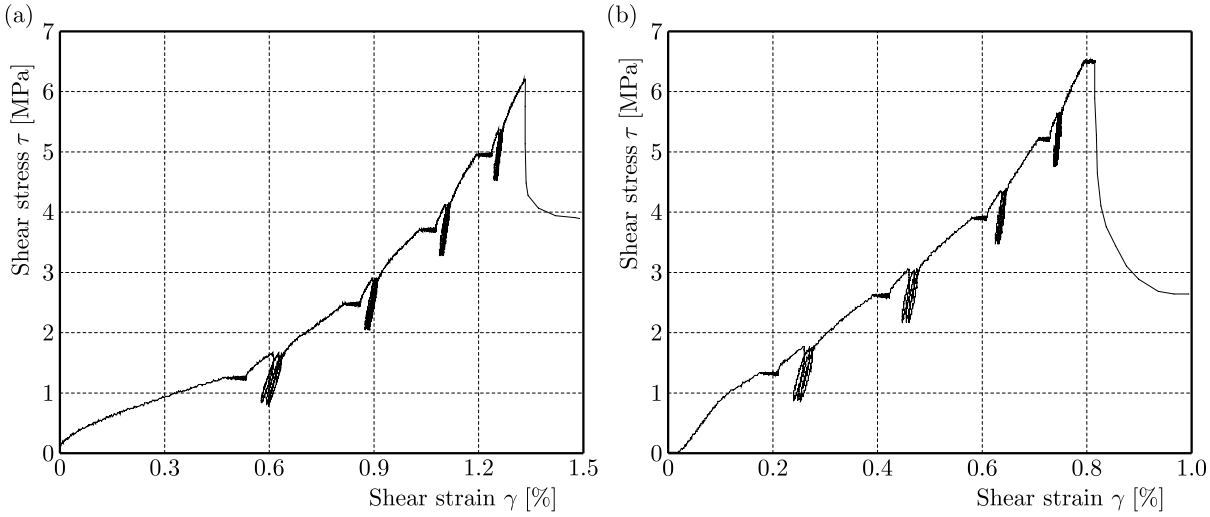

Fig. 5. Shear stress-strain curves under fatigue loading: (a) sandstone, (b) marble

4. Nonlinear model

4.1. Creep body

The above research shows that the shear creep curve under fatigue loading has a typical acceleration stage, and its nonlinear characteristics are obvious. On the whole, compared with the final damage, the creep curve under fatigue loading fluctuates less, and the influence of fatigue loading on the creep curve is mainly considered to be the influence after fatigue loading, which is a simplified treatment. A creep model mainly produces the creep curve after eliminating the fluctuation in data, so a new nonlinear creep body is introduced (Lian *et al.*, 2020) in this paper, which is composed of a variable-section Newton damper, as shown in Fig. 6a.

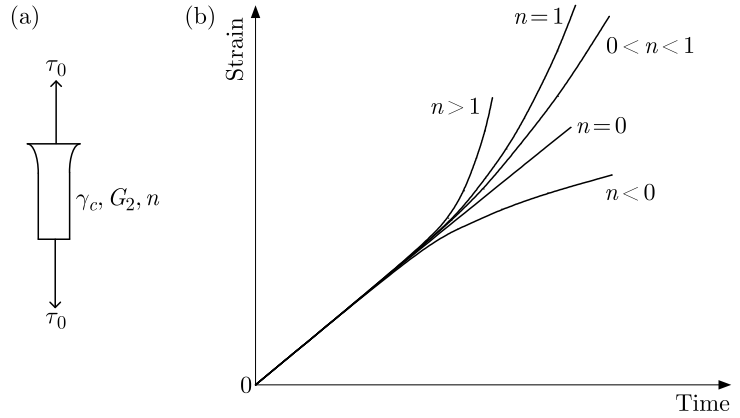

Fig. 6. Creep model: (a) creep body, (b) creep curve

The creep can be divided into two phases according to mechanical characteristics of the rock:
— mechanical properties of the linear phase of creep (Liu and Zhang, 2020; Su *et al.*, 2016)

$$\frac{d\gamma}{dt} = \frac{\tau}{G_2} \tag{4.1}$$

— mechanical properties of creep in the nonlinear stage (Jowkar *et al.* 2020)

$$\frac{d\gamma}{dt} = \frac{\tau}{G_2}\left(\frac{\gamma}{\gamma_c}\right)^n \tag{4.2}$$

where γ_c, G_2 and n are model parameters.

When the shear stress is constant, i.e., $\tau = \tau_0$, the creep state equations are as follows (Duan *et al.*, 2020)

$$\gamma = \frac{\tau_0}{G_2} t \qquad 0 \leqslant t < t_c \tag{4.3}$$

and for $t_c \leqslant \infty$

$$\gamma = \begin{cases} \exp\Big(\dfrac{\tau_0}{\gamma_c G_2} t + \ln \gamma_c - 1\Big) & \text{for} \quad n = 1 \\ \gamma_c \Big[\dfrac{(1-n)\tau_0}{\gamma_c G_2} t + n\Big]^{\frac{1}{1-n}} & \text{for} \quad n \neq 1) \end{cases} \tag{4.4}$$

where γ is the shear strain; τ_0 is the shear stress, MPa; t_c is the transition point between the linear and nonlinear stage h; that is, the starting point of the acceleration stage in the creep curve.

The creep curve is shown in Fig. 6b: When $n \leqslant 1$, if time tends to be infinite, the shear strain tends to be infinite, and the specimen is damaged, corresponding to the situation in which the creep failure of rock occurs after a long time due to the low stress level in actual creep. When $n > 1$, the shear strain tends to be infinite when $t = t_p$, and the specimen is damaged. t_p is the time to creep failure. This corresponds to failure of rock within a limited time due to a high stress level. The model can represent different types of rock due to different values of n and can be used in practice. The creep can be described as Y body.

4.2. Nonlinear rheological model

The rheological process of rock is a complex process in which elastic, plastic, viscoelastic, viscoplastic and other types of deformation coexist, so the combination of multiple elements is generally used for simulation. In this paper, the Hooke body (H body), Kelvin body (K body) and creep (Y body) are combined in series to form a composite nonlinear model, in which the Hooke body simulates elasticity of the rock, the Kelvin body simulates viscoelasticity of the rock, and the linear and nonlinear stages in the Y body are used to simulate constant velocity creep deformation and accelerated creep deformation of the rock, respectively. This model is shown in Fig. 7.

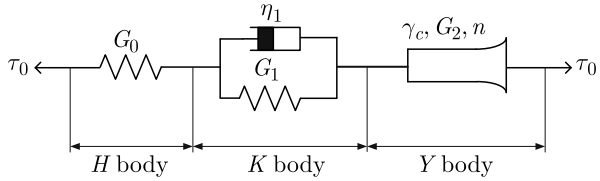

Fig. 7. Nonlinear model

According to the series rule, the creep equation of the model is obtained as follows (Bandyopadhayay *et al.*, 2020; Zuo *et al.*, 2019):
— when $0 \leqslant t < t_c$

$$\gamma = \frac{\tau_0}{G_0} + \frac{\tau_0}{G_1}\Big[1 - \exp\Big(-\frac{G_1}{\eta_1} t\Big)\Big] + \frac{\tau_0}{G_2} t \tag{4.5}$$

— when $t_c < t \leqslant t_p$

$$\gamma = \begin{cases} \dfrac{\tau_0}{G_0} + \dfrac{\tau_0}{G_1}\Big[1 - \exp\Big(-\dfrac{G_1}{\eta_1} t\Big)\Big] + \dfrac{\tau_0}{G_2} t + \exp\Big(\dfrac{\tau_0}{\gamma_c G_2} t + \ln \gamma_c - 1\Big) & \text{for} \quad n = 1 \\ \dfrac{\tau_0}{G_0} + \dfrac{\tau_0}{G_1}\Big[1 - \exp\Big(-\dfrac{G_1}{\eta_1} t\Big)\Big] + \dfrac{\tau_0}{G_2} t + \gamma_c \Big[\dfrac{(1-n)\tau_0}{\gamma_c G_2} t + n\Big]^{\frac{1}{1-n}} & \text{for} \quad n \neq 1 \end{cases} \tag{4.6}$$

where G_0 is the shear modulus of the Hooke body, GPa; G_1 is the shear modulus of the Kelvin body, GPa; and η_1 is the viscosity coefficient of the Kelvin body, GPa·h.

5. Model validation

5.1. Solution of model parameters

To find for the relevant parameters of the creep equation, the creep test data of sandstone and marble are combined with the nonlinear least square method of Origin software (Smith *et al.*, 2019). Thus, the creep model equation proposed in this paper is customized, and the final model parameters are obtained through inversion, as shown in Table 2. Table 2 shows that the fitting coefficients of soft rock and hard rock are higher than 0.94, indicating that the fitting degree is good.

Table 2. Summary of model parameters

Sample	Shear stress [MPa]	G_0 [GPa]	G_1 [GPa]	G_2 [GPa]	η_1 [GPa·h]	γ_c	n	R^2
Sandstone	1.5	1.78	1.41	24.41	11.54	–	–	0.98
	3.0	1.45	1.17	19.17	10.43	–	–	0.98
	4.5	0.95	0.52	18.52	9.77	–	–	0.97
	6.0	0.87	0.42	17.23	8.34	–	–	0.96
	6.2	0.86	0.24	15.24	8.12	0.51	2.58	0.94
Marble	1.5	2.73	2.97	34.97	17.46	–	–	0.98
	3.0	2.35	2.22	28.22	16.32	–	–	0.97
	4.5	2.22	2.16	26.56	12.44	–	–	0.96
	6.0	2.03	2.10	22.44	10.23	–	–	0.95
	6.5	1.88	1.94	18.94	8.82	0.32	1.66	0.94

5.2. Model validation

Comparing the theoretical equation with the experimental data, the results are shown in Fig. 8, in which the circular data points represent the experimental data under different stress levels, and the solid line represents the calculated theoretical results.

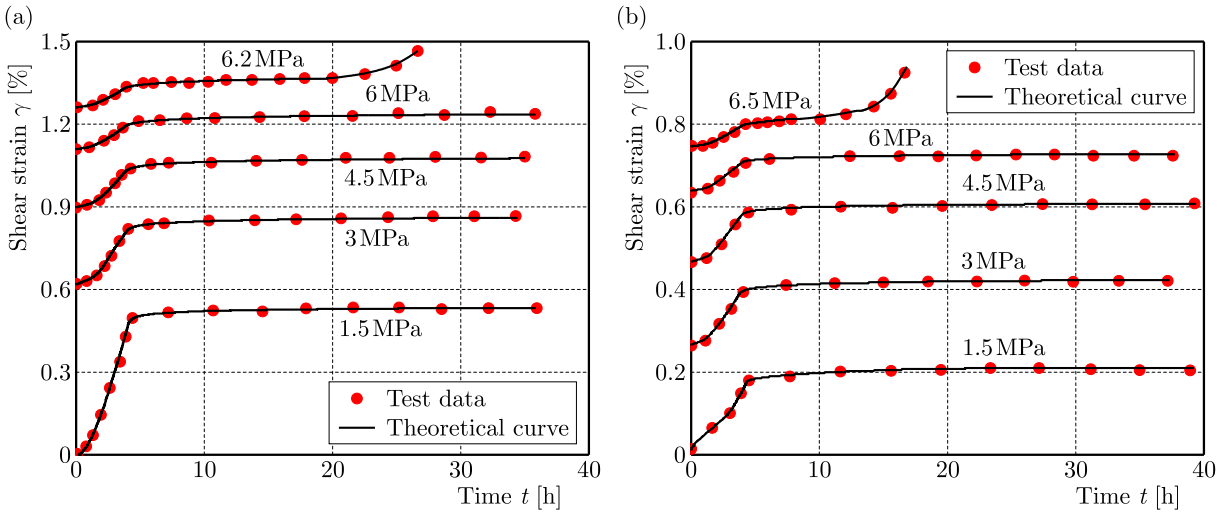

Fig. 8. Comparison between experimental data and theoretical curves: (a) sandstone, (b) marble

Clearly, the theoretical curves can accurately describe the creep test data of the sandstone and marble, which indicates that the model is suitable for both soft rock and hard rock and that the model can accurately reflect the shear deformation and mechanical characteristics of an anchored rock mass under fatigue loading. The shear creep process is accompanied by a change in the mechanical properties of the specimen, which also shows that the model has a wide range of applicability.

6. Conclusion

Based on the shear creep testing of sandstone and marble under fatigue loading, this paper explores the influence of fatigue loading on the shear creep of soft rock and hard rock.

- The creep curves and creep fatigue curves show clear creep characteristics, including instantaneous creep, decay creep, steady-state creep and accelerated creep. Compared with the creep observed without fatigue loading, the creep damage of sandstone and marble under fatigue loading increases by 12.8% and 21.9%, respectively, indicating that deformation of hard rock is more sensitive to fatigue loading.
- Sandstone creeps more than marble under fatigue loading, approximately 1.6 times more. Therefore, the lower the rock strength is, the more obvious its rheological properties are. The residual strength of sandstone is greater than that of marble, approximately 1.5 times greater.
- Under the same rock strength, the isochronal shear modulus gradually decreases with increasing time. With increasing shear stress, the fluctuation in the creep under fatigue loading presents a gradual decreasing trend. This is because an increase in shear stress increases the degree of internal pore closure of a specimen in the steady-state stage, which leads to a further decrease in the degree of internal pore closure during fatigue loading. Thus, the fluctuation in the creep decreases during fatigue loading.
- A new nonlinear rheological model of rock is constructed by including creep, which describes nonlinear characteristics of rock, with the existing model. The accuracy of the new model is verified by experimental data, which provides a reference for the support of surrounding rock under fatigue loading.

Acknowledgments

The research described in this paper was financially supported by the National Natural Science Foundation (51974146, 52174078), Liaoning Natural Science Foundation (2019-ZD-0042), Innovative Talents Support Program for Universities in Liaoning Province (21-1071) and Discipline Innovation Team of Liaoning Technical University (LNTU20TD08).

References

1. Bandyopadhayay K., Mallik J., Ghosh T., 2020, Dependence of fluid flow on cleat aperture distribution and aperture-length scaling: a case study from Gondwana coal seams of Raniganj Formation, Eastern India, *International Journal of Coal Science and Technology*, **7**, 1, 133-146
2. Duan Y., Wang S., Wang W., Zheng K., 2020, Atmospheric disturbance on the gas explosion in closed fire zone, *International Journal of Coal Science and Technology*, **7**, 4, 752-765
3. Feng F., Chen S., Zhao X., Li D., Wang X., Cui J., 2022, Effects of external dynamic disturbances and structural plane on rock fracturing around deep underground cavern, *International Journal of Coal Science and Technology*, **9**, 1, 15-27

4. Hu B., Yang S., Xu P., Tian W., 2019, Time-scale effect of the creep model parameters and particle flow simulation of sandstone with a single crack, *Chinese Journal of Geotechnical Engineering*, **41**, 5, 864-873

5. Huang M., Jiang Y., Wang S., Deng T., 2017, Identification of the creep model and its parameters of soft rock on the basis of disturbed state concept, *Chinese Journal of Solid Mechanics*, **38**, 6, 570-578

6. Jangara H., Ozturk C.A., 2021, Longwall top coal caving design for thick coal seam in very poor strength surrounding strata, *International Journal of Coal Science and Technology*, **8**, 4, 641-658

7. Jierula A., Oh T.-M., Wang S., Lee J., Kim H., Lee J., 2021, Detection of damage locations and damage steps in pile foundations using acoustic emissions with deep learning technology, *Frontiers of Structural and Civil Engineering*, **15**, 2, 318-332

8. Jowkar A., Sereshki F., Najafi M., 2020, Numerical simulation of UCG process with the aim of increasing calorific value of syngas, *International Journal of Coal Science and Technology*, **7**, 196-207

9. Lian X.G., Hu H.F., Li T., Hu D., 2020, Main geological and mining factors affecting ground cracks induced by underground coal mining in Shanxi Province, China, *International Journal of Coal Science and Technology*, **7**, 2, 362-370

10. Liu W., Zhang S., 2020, Research on rock creep model based on dual effects of stress and time, *Journal of Central South University*, **51**, 8, 2256-2265

11. Luo F., Zhang y., Zhu Z., 2020, Creep constitutive model for frozen sand of Qinghai-Tibet Plateau, *Journal of Harbin Institute of Technology*, **52**, 2, 26-32

12. Małkowski P., Niedbalski Z., Balarabe T., 2021, A statistical analysis of geomechanical data and its effect on rock mass numerical modeling: a case study, *International Journal of Coal Science and Technology*, **8**, 2, 312-323

13. Nádudvari Á., Abramowicz A., Fabiańska M., Misz-Kennan M., Ciesielczuk J., 2021, Classification of fires in coal waste dumps based on Landsat, Aster thermal bands and thermal camera in Polish and Ukrainian mining regions, *International Journal of Coal Science and Technology*, **8**, 3, 441-456

14. Smith J.A., Ramandi H.L., Zhang C., Timms W., 2019, Analysis of the influence of groundwater and the stress regime on bolt behaviour in underground coal mines, *International Journal of Coal Science and Technology*, **6**, 2, 286-300

15. Song Z., Ji H., Liu Z., Sun L., 2020, Study on the critical stress threshold of weakly cemented sandstone damage based on the renormalization group method, *International Journal of Coal Science and Technology*, **7**, 4, 693-703

16. Su G., Hu L., Feng X., 2016, True triaxial experimental study of rockburst process under low frequency cyclic disturbance load combined with static load, *Chinese Journal of Rock Mechanics and Engineering*, **35**, 7, 1309-1322

17. Sun J., 2007, Rock rheological mechanics and its advance in engineering applications, *Chinese Journal of Rock Mechanics and Engineering*, **26**, 6, 6-31

18. Szkudlarek Z., Janas S., 2021, Active protection of work area against explosion of dust–gas mixture, *International Journal of Coal Science and Technology*, **8**, 4, 674-684

19. Valiulin S.V., Onischuk A.A., Baklanov A.M., Bazhina A.A., Paleev D.Yu., Zamashchikov V.V., Korzhavin A.A., Dubtsov S.N., 2020, Effect of coal mine organic aerosol on the methane/air lower explosive limit, *International Journal of Coal Science and Technology*, **7**, 4, 778-786

20. Wang C., Chen L., Liang J., 2014, Creep constitutive model for full creep process of granite considering thermal effect, *Rock and Soil Mechanics*, **35**, 9, 2493-500+506

21. Wei L., Zhu Z., Meng Q., 2019, Dynamic characteristics of marble damaged by cyclic loading, *Explosion and Shock Waves*, **39**, 8, 63-73

22. Wiatowski M., Muzyka R., Kapusta K., Chrubasik M., 2021, Changes in properties of tar obtained during underground coal gasification process, *International Journal of Coal Science and Technology*, **8**, 5, 1054-1066

23. Yu J., Li T.-B., Zhang J.-Z., Cai Y., 2014, Stress characteristics of surrounding rocks for inner water exosmosis in high-pressure hydraulic tunnels, *Journal of Central South University*, **21**, 7, 2970-2976F

24. Zhu Z., Feng T., Gong F., 2016, Experimental research of mechanical properties on grading cycle loading-unloading behavior of coal-rock combination bodies at different stress levels, *Journal of Central South University*, **47**, 7, 2469-2475

25. Zuo J., Zhou Y., Liu G., 2019, Continuous deformation law and curvature model of rock strata in coal backfill mining, *Rock and Soil Mechanics*, **40**, 3, 1097-1104

Manuscript received May 1, 2022; accepted for print July 26, 2022